ACS APPLIED MATERIALS & INTERFACES

Forum Article

www.acsami.org

Solvent Vapor Annealing in the Molecular Regime Drastically Improves Carrier Transport in Small-Molecule Thin-Film Transistors

Hadayat Ullah Khan,[†,‡] Ruipeng Li,[†,‡] Yi Ren,[†] Long Chen,[†] Marcia M. Payne,[⊥] Unnat S. Bhansali,[†] Detlef-M. Smilgies,[§] John E. Anthony,[⊥] and Aram Amassian*[,†]

[†]Physical Sciences and Engineering Division, King Abdullah University of Science and Technology, Thuwal 23955-6900, Saudi Arabia

[§]Cornell High Energy Synchrotron Source, Cornell University, Ithaca, New York 14850, United States

[⊥]Department of Chemistry, University of Kentucky, Lexington, Kentucky 40506, United States

Supporting Information

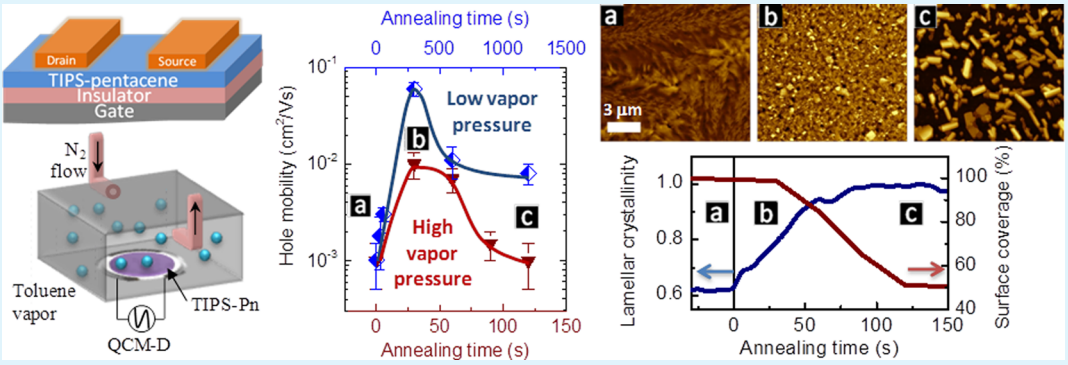

ABSTRACT: We demonstrate a new way to investigate and control the solvent vapor annealing of solution-cast organic semiconductor thin films. Solvent vapor annealing of spin-cast films of 6,13-bis(triisopropylsilylethynyl) pentacene (TIPS-Pn) is investigated in situ using quartz crystal microbalance with dissipation (QCM-D) capability, allowing us to monitor both solvent mass uptake and changes in the mechanical rigidity of the film. Using time-resolved grazing incidence wide angle X-ray scattering (GIWAXS) and complementary static atomic force microscopy (AFM), we demonstrate that solvent vapor annealing in the molecular regime can cause significant performance improvements in organic thin film transistors (OTFTs), whereas allowing the solvent to percolate and form a liquid phase results in catastrophic reorganization and dewetting of the film, making the process counterproductive. Using these lessons we devise processing conditions which prevent percolation of the adsorbed solvent vapor molecules for extended periods, thus extending the benefits of solvent vapor annealing and improving carrier mobility by nearly two orders of magnitude. Ultimately, it is demonstrated that QCM-D is a very powerful sensor of the state of the adsorbed solvent as well as the thin film, thus making it suitable for process development as well as in-line process monitoring both in laboratory and in future manufacturing settings.

KEYWORDS: *organic electronics, organic thin film transistors, solvent vapor annealing, quartz crystal microbalance with dissipation, TIPS-pentacene, solution processing*

INTRODUCTION

Organic semiconductors have shown tremendous promise for a variety of applications in electronic and optoelectronic components and devices, including organic light-emitting diodes (OLEDs),[1] organic photovoltaics,[2] radio-frequency identification cards (RFIDs),[3,4] and biosensors.[5−7] The rapid progress of the field benefits from improvements in fabrication processes − namely solution processing and post-processing, such as thermal and solvent vapor annealing − and new material designs, leading to notable performance improvements in the electronic and transport properties of organic semiconducting materials.[8−11] Organic thin-film transistors (OTFTs) have gained considerable attention due to their low cost, ease of manufacturing, compatibility with flexible, large-area substrates, and numerous demonstrations of scalable patterning processes.[12−14] Ecological and economical solution-based methods seem to be highly encouraging because of the relatively simple processes involved and the reduced requirements in terms of facilities. Nonetheless, these soluble polymers or small molecules require subsequent chemical and/or thermal processing/treatment after deposition to optimize electronic properties.

Special Issue: Forum on Advancing Technology with Organic and Polymer Transistors

Received: October 30, 2012
Accepted: January 26, 2013
Published: February 8, 2013

Long-range molecular order, surface coverage, and continuity[15] and minimal density of grain boundaries exhibiting large crystallographic misorientation[16] are important to achieving high-performance small-molecule-based OTFTs.[17−19] As such, there is a pressing need for simple methods that increase crystallinity and enhance growth of ordered domains in as-deposited, solution-cast organic semiconductors without compromising film continuity via dewetting or causing formation of polymorphs unfavorable to efficient in-plane carrier transport.[20,21] Solvent vapor annealing and related methods have emerged in recent years as convenient, low-temperature methods of tuning material structure and thus device performance, by allowing the kinetically trapped thin film prepared by methods such as spin-casting or inkjet printing to approach thermodynamic equilibrium by enabling reorganization and mass transport of the molecular building blocks of the film.[22−28] Studies reported to date have relied mainly on trial-and-error methods to optimizing conditions effective in improving the performance of devices, in large part because of the difficulties associated with quantifying the uptake of solvent molecules by the semiconductor thin film and then measuring the effects of the solvent molecules as they modify the structure and morphology of thin films. Post-deposition studies are quite useful, but they do not provide any direct evidence as to the amount of solvent vapor uptake, mechanisms of solvent-film interactions or the state of the film during exposure to solvent vapor molecules.

Here, we demonstrate a new method based on the use of a quartz crystal microbalance with dissipation (QCM-D) measurement capability to identify optimal solvent vapor annealing conditions for small-molecule semiconductor-based OTFTs. The QCM-D technique has been widely used for in situ monitoring of adsorption on the surface of a quartz crystal immersed in a liquid medium. QCM-D has been applied to a broad range of material systems, including polymers,[29] proteins,[30] nanoparticles,[31] and more recently to investigate dye adsorption in dye-sensitized solar cells[32] and nucleation and growth of small-molecule thin films during solution drying.[33] QCM-D allows sensitive quantification of solvent vapor uptake as well as a measure of the mechanical properties of the film in the presence of the adsorbed solvent, and has been recently used to investigate and control nucleation of small-molecule thin films at the solid−liquid interface during solution processing.[33] The ability to sense changes in the mechanical properties of the film and adsorbate can reveal the effect of solvent molecules on the film. The QCM-D analysis is complemented by time-resolved grazing incidence wide-angle X-ray scattering (GIWAXS) to track the microstructure and texture of the as-cast film, while also relying on atomic force microscopy (AFM) to follow the evolution of thin film morphology and surface coverage. Our study suggests that solvent vapor annealing in the molecular regime, i.e., while the solvent molecules are still isolated, is very effective at improving carrier transport and device performance by promoting lamellar crystallization in the kinetically trapped spin-cast film, whereas allowing the solvent molecules to percolate and form a liquid − either by excessive vapor supply (saturation vapor annealing) or extended vapor-surface interaction time − dramatically degrades device performance primarily via dewetting of the film. Insight from the various in situ metrology techniques reveals that crystallization and dewetting can be decoupled by controlling the dose and duration of solvent vapor annealing. Using these lessons, we demonstrate that carrier mobility of spin-cast films of 6,13-bis(triisopropylsilylethynyl) pentacene (TIPS-Pn) can be improved by nearly two orders of magnitude simply by maintaining the adsorbed solvent molecules in the molecular regime, thus preventing large scale dewetting from occurring. These results suggest that QCM-D could be used in-line to monitor drop-casting[33] or solvent vapor annealing the same way that QCM has become a mainstay for deposition rate monitoring in vacuum processing of thin films.

EXPERIMENTAL SECTION

Materials. 6,13-Bis(triisopropylsilylethynyl) pentacene (TIPS-Pn) was synthesized by the Anthony group and used without further purification. Toluene (99.8% anhydrous) was purchased from Sigma-Aldrich and used witout further purification.

Device Fabrication and Characterization. Highly doped n-type single-crystal silicon (100) wafers with a 300 nm thermal oxide film were used for fabrication of top-contact, bottom-gate OTFTs. The substrates were cleaned by rinsing in acetone, isopropanol, ethanol, and de-ionized (DI) water followed by Standard Clean 1 (RCA) ammonium hydroxide (30% NH_4OH), hydrogen peroxide (30% H_2O_2) and DI water (with 1:1:5 ratio) for 30 min at 70 °C. All substrates were dried with N_2 and annealed at 100 °C for 10 min. A 1 wt % solution of TIPS-Pn in toluene was spin-cast onto the substrate or sensor at 1000 rpm for 30 s. No further annealing was performed. Gold source-drain electrodes were evaporated through a shadow mask with a channel width (W) of 500 μm and length (L) of 60 μm. All electrical measurements were performed with a Keithley 4200 Semiconductor Characterization System inside a nitrogen glove box.

Characterization. The thicknesses of SiO_2 and of as-cast films of TIPS-Pn were measured using variable angle spectroscopic ellipsometry (VASE, M-2000XI, J. A. Woollam. Co, Inc.). Thin film thickness was found to be highly reproducible and ranged between 49 and 51 nm. The surface morphology was analysed by atomic force microscopy (AFM; Agilent 5400 SPM) and polarized optical microscopy (Nikon LV100 POL) before solvent vapor annealing as well as after specific annealing times.

QCM-D. QCM-D (Q-sense, Biolin Scientific) was used to monitor solvent vapor annealing by using quartz sensors pre-coated with SiO_2 (by sputtering) and subsequently coated by a spin-cast layer of TIPS-Pn. The sensor of QCM-D is an AT-cut piezoelectric quartz crystal with an active area of 12 mm^2, coated with a 10 nm Au layer and terminated with a 100 nm thick SiO_2 layer, exhibiting a root mean squared surface roughness of ∼1 nm, as determined by AFM. The sensor undergoes shear oscillation with a fundamental frequency of 5 MHz and odd overtones (n = 3, 5, 7, ...) when an electric field is applied. In traditional QCM, the resonance frequency of the oscillating crystal changes (ΔF) in response to mass change (Δm) on the surface (adsorption, desorption, deposition, etching, etc.) and is related by the Sauerbrey equation,[34] $\Delta m = -((t_q\rho_q)/f_0 n)\Delta F$, where t_q is the thickness of quartz, ρ_q is the density of quartz, f_0 is the resonance frequency, and n is the harmonic number; note that $\Delta F < 0$ when $\Delta m > 0$. The Sauerbrey relationship holds assuming the adsorbed mass is (1) small relative to the mass of the crystal, (2) rigid and rigidly bound to the surface of the crystal, and (3) evenly distributed across the surface of the crystal. For systems incorporating both viscous and elastic responses, typical of soft matter, the assumptions of the Sauerbrey model are violated. The dissipation D is related to the viscoelastic properties of the film, defined as $D = (E_{lost}/2\pi E_{system})$, where E_{lost} is the energy lost in every oscillation and E_{system} is the total energy of the system. QCM-D measures the change in dissipation (ΔD) due to viscoelastic response of the adsorbed mass by applying a pulsed driving voltage and monitoring the decay of the shear oscillations between successive pulses. Simultaneous, fast measurements of ΔF and ΔD are therefore possible for all overtones at a sampling rate of up to 200 Hz. The resolutions of ΔF and ΔD in liquid media are ±0.1 Hz and $\pm 1 \times 10^{-7}$, respectively, equivalent to ng/cm^2 in terms of mass sensitivity. Typical experiments are performed at a rate of 10 Hz, fast enough to monitor most processes while achieving good signal-to-noise ratio. The viscoelastic properties of a given film

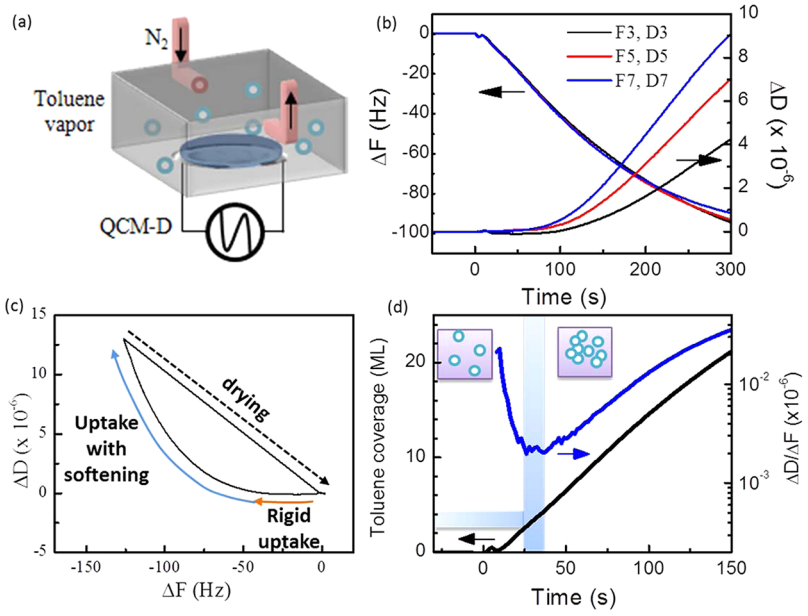

Figure 1. In situ QCM-D measurements during solvent vapor annealing on quartz sensors coated via spin-casting with a TIPS-Pn thin film. (a) Schematics of an environmental chamber holding the quartz crystal, (b) ΔF and ΔD versus solvent vapor annealing time in saturated toluene atmosphere at room temperature. (c) ΔD vs. ΔF trajectory plot. (d) Toluene uptake measured in terms of surface coverage in units of ML and corresponding $\Delta D/\Delta F$ (blue curve) showing changes in rigidity per unit mass adsorbed onto the film. Insets in (d) illustrate the molecular and percolated regimes of solvent vapor on the surface of the sample.

can be qualitatively assessed by calculating $\Delta D/\Delta F$, with small values indicating a more rigid film. The film can be considered rigid for $\Delta D/\Delta F < 2\times10^{-7}$ s. Viscous response is also qualitatively indicated by the splitting of overtones of ΔF and ΔD because of frequency-dependence of viscoelastic properties.[35] In these highly dissipative systems, it is necessary to use the more complex Voigt model for estimating the thickness and viscoelastic properties of the layer.[6]

Experiments are initiated by loading the TIPS-Pn-coated sensors into the sensor holder, which is mounted in a custom-built environmental chamber with solvent reservoir, solvent injection mechanism and inert gas flow tubes with flow controllers. Upon achieving a stable baseline with N_2 flowing at high rate, so as to prevent any detectable solvent vapor build-up, we inject 100 μL of toluene into the solvent reservoir and adjust the N_2 flow rate to tune the solvent vapor build-up in the chamber at room temperature. We monitor changes in frequency (ΔF) and dissipation (ΔD) of the 3rd, 5th, and 7th overtones and apply the Sauerbrey analysis to the 3rd overtone so as to estimate the mass and approximate coverage of toluene using the volume density and molar density of liquid toluene at room temperature, and assuming an isotropic molecular shape for toluene.

In situ grazing incidence wide-angle x-ray scattering (GIWAXS) measurements were carried out at D-line (Cornell High Energy Synchrotron Source). A 0.5 × 0.1 mm beam with a wavelength of 1.23 Å and wide band pass (1.47%) was generated from double-bounce multilayer monochromator. The incidence angle was 0.15° with respect to the substrate plane, as established by performing X-ray reflectivity using an ion chamber. A 50 × 50 mm^2 CCD area detector (Medoptics) with pixel size of 46.9 μm was placed at a distance of 92 mm from the sample stage. A 1.5 mm wide tantalum rod was used to block the intense scattering at low angles of incidence. GIWAXS images were acquired at a rate of 1 image every 6 s, with 1 s integration time and 5 s readout time. During X-ray scattering experiments samples were kept in a chamber with vapor pressure control and Kapton windows to allow X-ray scattering through the chamber: liquid solvent was injected into a reservoir at the bottom of the cell; a purge gas flow of dry nitrogen established a vapor pressure that could be regulated from almost zero to equilibrium vapor pressure of the solvent.[24] Experimental conditions at the synchrotron were kept identical to the QCM-D experiments performed at KAUST.

RESULTS AND DISCUSSION

Quartz crystal microbalance with dissipation (QCM-D) measurements are intended to shed light on solvent uptake and solvent-film interactions. For this purpose, TIPS-Pn thin films were spin-cast on the SiO_2-coated quartz sensor prior to mounting the sensors on the instrument contained inside a custom-built environmental chamber, schematically illustrated in Figure 1a. QCM-D measures the change of resonance frequency (ΔF) of the AT-cut quartz crystal caused by a change in mass bound to the surface of the crystal (e.g., $\Delta F < 0$ in case of solvent uptake or $\Delta F > 0$ in case of solvent desorption), as well as the energy dissipation (ΔD), which relates to the amount of energy lost per cycle of shear oscillation of the quartz sensor by virtue of changing viscoelastic properties of the bound mass (e.g., $\Delta D \approx 0$ if the film and adsorbed solvent molecules behave rigidly, $\Delta D > 0$ if the film softens and/or solvent liquid forms).[36,37]

To initiate the QCM-D experiments, we inject a small volume of solvent into a reservoir within the environmental chamber and measure ΔF and ΔD, as shown in Figur 1b. There is no flow of nitrogen in these initial experiments so as to achieve the saturation regime of toluene under normal circumstances. ΔF decreases sharply in the first 1−2 min and resembles an exponential decay approaching saturation within ~5 min. Meanwhile, $\Delta D \approx 0$ during the initial minute but increases gradually while ΔD overtones also split. The splitting of overtones is common in case of significant softening, indicating formation of liquid upon the surface. In Figure 1c, we show the ΔD vs ΔF trajectory plot to reveal the various stages of mass uptake and state of the film during solvent vapor annealing. Initially, the film takes up solvent while remaining rigid, followed by significant softening. The experiment is completed as solvent vapor is removed quickly by flowing nitrogen through the environmental chamber at high flow rate. These results highlight the presence of a significant process

dx.doi.org/10.1021/am3025195 | ACS Appl. Mater. Interfaces 2013, 5, 2325−2330

window whereby solvent uptake is possible without softening or partially dissolving the film. To monitor the effect of solvent uptake more sensitively, we plot $\Delta D/\Delta F$ vs time and the amount of toluene uptake in terms of surface coverage with units of monolayer (ML) in Figure 1d. Interestingly, we find that uptake of the first 1−2 monolayers of toluene by the 50 nm film of TIPS-Pn reduces $\Delta D/\Delta F$ by an order of magnitude, indicating that toluene does not soften the film nor does it nucleate to form a liquid mass on the surface during the initial 25−30 s of the vapor exposure process. We refer to this regime as the molecular regime, whereby toluene molecules are present on the surface, at grain boundaries and in the bulk of the film mainly as isolated molecules. A turnaround in $\Delta D/\Delta F$ is detected when toluene uptake reaches 3-4 ML, suggesting softening action by the solvent molecules. We argue that this corresponds to the nucleation of liquid solvent, whereby toluene molecules cluster together on the surface and at grain boundaries. This mechanism will be substantiated using in situ GIWAXS (see below). For $t > 40$ s, $\Delta D/\Delta F$ rises monotonously as more and more solvent is taken up by the film softening.

Let us now find out how QCM-D measurements of solvent vapor uptake and rigidity/softening correlate with actual changes in the morphology and microstructure of spin-cast TIPS-Pn films. AFM topography image series of the surface of TIPS-Pn films are shown in Figure 2a−f. Polarized optical micrographs are shown in Figure S1 in the Supporting Information for the same films. The as-cast film exhibits a dendritic morphology with fine domains covering the entire surface of the substrate. At 30 s, the film undergoes significant transformation, as indicated by formation of a large number of uniformly sized crystallites with very good connectivity and surface coverage. This suggests that a very small dose of solvent vapor in the molecular regime is capable of dramatically transforming the morphology of the film. Further exposure of the film to solvent vapor leads to significant coarsening by virtue of the increase of the lateral size of features (see c and d), but also to formation of a binomial population of flat features, presumably from the original film, as well as clusters of tall and highly isolated crystallites with regular shape and sharp corners. Formation of tall, isolated crystallites suggests both intra and intergrain mass transport and is partly associated to dewetting of the film from the substrate.[24] As solvent vapor annealing proceeds further, there appears to be full transformation of the continuous film into a series of tall, isolated crystallites, as shown in e and f. Aggregation of these crystallites at long exposure times (f) suggests the presence of significant liquid solvent, which can cause the large crystallites to migrate and cluster together on the surface of the substrate. From histograms of the distribution of surface height, we estimate the fractional surface coverage associated to the original film, formation of tall crystallites and substrate exposure, as shown in Figure 2g. Clearly, surface coverage remains unperturbed only for a vapor treatment of 30 s or less in saturation environment.

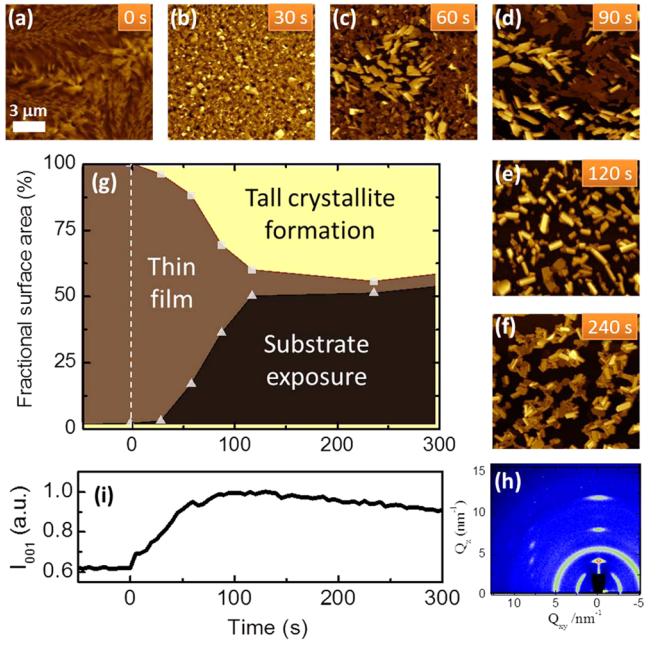

Figure 2. Influence of solvent vapor annealing in saturation regime of toluene on the morphology and microstructure of TIPS-Pn thin films. (a−f) AFM images (20 × 20 μm^2) taken at different annealing times. (g) Fractional surface coverage by thin film crystallites, tall crystallites, and bare substrate with respect to annealing time, calculated from histograms of surface height from AFM. (h) GIWAXS pattern of TIPS-Pn film after vapor annealing, showing Bragg sheets ($Q_{xy} = 0$) and Bragg peaks ($Q_{xy} \approx 8$ nm^{-1}) and diffraction rings originating from the Kapton windows of the chamber. (i) Time-dependence of the (001) Bragg sheet intensity of TIPS-Pn with respect to process time.

Interestingly, the TIPS-Pn crystallites do not dissolve appreciably during the exposure to solvent vapor, as indicated by time-resolved GIWAXS measurements (h and i). By monitoring the lamellar Bragg sheet $(001)_{BS}$, we find increasing diffraction signal from 0 to 100 s, followed by a slight and slow decay of lamellar crystallinity, suggesting some loss of long range order due to the presence of large quantities of solvent (see Figure 1d). It is noteworthy that crystallization continues past 25−30 s, even as QCM-D revealed an onset of softening and found this to correlate with the onset of significant reorganization and dewetting of the film. This proves that softening detected by QCM-D is associated to the formation of the liquid state of solvent on the surface rather than to any significant dissolution of the TIPS-Pn film.

Reasonable extrapolation can be made about the impact of structural and morphological changes reported in Figure 2 on the performance of OTFTs films. On one hand, increasing lamellar crystallinity and texture should promote intragrain carrier transport; on the other hand, dewetting of the film and loss of continuous pathways is expected to act as a major barrier to intergrain carrier transport required to connect the source and drain electrodes. In Figure 3, we track (a) the carrier mobility, (b) on-off ratio and threshold voltage with respect to solvent vapor exposure time for the same films featured in Figure 2. For comparison, we also plot $\Delta D/\Delta F$ vs time in a. It is remarkable that the average carrier mobility increases by an order of magnitude from ~1 × 10^{-3} to ~1 × 10^{-2} cm^2/(V s) during solvent uptake in the molecular regime and subsequently decreases − slowly at first as the solvent nucleates but then quite rapidly − to ~1 × 10^{-3} cm^2/(V s) and lower. The on-off ratio also rises by nearly an order of magnitude from ~3 × 10^3 to ~5 × 10^4. A change in the threshold voltage, V_{th}, is detected from +3 V to −6 V as a function of exposure time, which may be due to the changing microstructure and morphology of the film. These experiments demonstrate the significant benefits of solvent vapor annealing in the molecular regime on device performance by virtue of improvement of thin film microstructure.[38] However, as expected, the benefits of

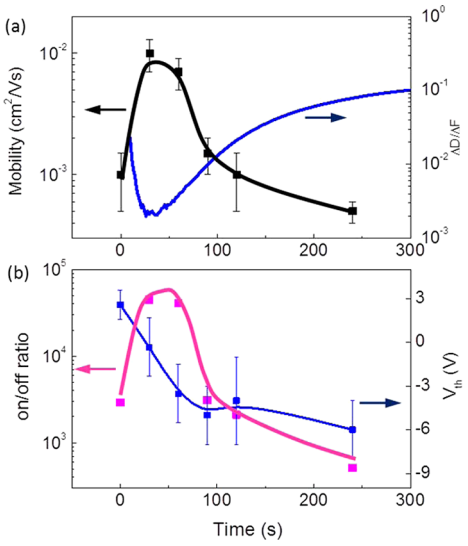

Figure 3. Electrical performance of bottom-gate/top-contact OTFTs of TIPS-Pn. All devices were fabricated on highly doped Si wafer with SiO_2 (300 nm) dielectric layer with a 50 nm thick spin-cast film of TIPS-Pn followed by Au source-drain electrode evaporation with a W/L of 8.34 and measured in a N_2 glove box. (a) Hole mobility (black curve) and $\Delta D/\Delta F$ (blue curve) with respect to annealing time. (b) Variation of on/off ratio and V_{th} as a function of annealing time. The error bar represents the variation from a minimum of 4 devices. The detailed transfer and output characteristics are shown in the Supporting Information, Figure S2.

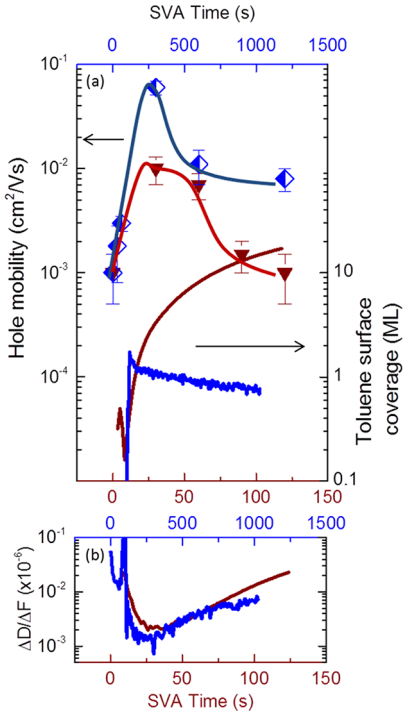

Figure 4. Electrical performance of top-contact TIPS-Pn OTFTs exposed to solvent vapor in the saturation (red) and low vapor pressure regimes (blue). Detailed transfer characteristics are shown in Figure S4 in the Supporting Information. (a) Hole mobility and toluene surface coverage and (b) $\Delta D/\Delta F$ with respect to annealing time.

crystallization are far outweighed by the deleterious action of liquid solvent upon the surface coverage of the thin film.[39]

Although the OTFT results reveal significant improvement within the first 30−60 s of the process with a peak performance around 30 s, the time-resolved GIWAXS analysis suggests significant room for further performance improvement if dewetting could somehow be avoided while structural changes are allowed to proceed. We have therefore set out to modify processing conditions so as to maintain the solvent uptake by the film to ≤2 ML of toluene. This was achieved by adjusting the flow rate of N_2 to 4 sccm through the environmental chamber, and is shown to limit the toluene uptake to just below 2 ML equivalent coverage thoughout the process, as verified by QCM-D (Figure 4a). In this case, the process is found to be nearly an order of magnitude slower, as revealed by the time scale of the low vapor pressure experiment in comparison to the saturation vapor experiment featured in Figures 1−3. In Figure 4a, we plot the average carrier mobility of TIPS-Pn OTFTs both in saturated vapor (data in red) and low vapor pressure (data in blue) conditions. There is a significant benefit in doing so, as revealed by the mean carrier mobility increase approaching two orders of magnitude within the first 300 s of the treatment, far surpassing the 10-fold increase seen in saturated vapor conditions. For extended treatment times, however, the mobility decreases to $\sim 1 \times 10^{-2}$ cm^2/(V s), which suggests some degree of degradation of film morphology. It is remarkable that even as the amount of solvent uptake is very low, solvent molecules can easily diffuse and have time to nucleate and grow given sufficient time, as indicated by the turnaround of $\Delta D/\Delta F$ around 200−300 s and subsequent monotonous increase. Indeed, AFM and polarized microscopy images in Figure S3 in the Supporting Information reveal mild reorganization of the film, which could lead to negative effects at grain boundaries. The effect is not as drastic as in the case of saturation vapor annealing conditions, but some of the benefit of vapor annealing in the molecular regime (t < 300 s) is nevertheless lost. These results suggest that maintaining the solvent vapor annealing conditions in the molecular regime is the most crucial criterium to extracting maximum benefit from the process. In addition, they demonstrate that process optimization should account for both solvent uptake and exposure time so as to maintain the adsorbed solvent in the molecular regime. This requirement appears to have some universality, as it is far more telling than the absolute amount of adsorbed solvent or the duration of the annealing process.

Above all, these results demonstrate that QCM-D is potentially an extremely powerful technique for use in organic electronics. One can envisage its use in the lab environment to help identify optimal conditions for a broad range of solvents and processing conditions without resorting systematically to performing costly and time-consuming experiments, such as device fabrication and/or thin film characterization for an endless combination of conditions. QCM-D also has the potential to be used in line with solution-based manufacturing processes requiring solvent vapor annealing to provide, for instance, real-time feedback to control processing conditions and achieve optimal OFET performance consistently.

CONCLUSION

Solvent vapor annealing is increasingly prevalent in organic electronics and beyond. However, much of the investigation into this process has thus far focused on trial and error, whereby samples are exposed under varying process conditions and durations and thin film structure and device performance are measured providing feedback to the process. In situ

dx.doi.org/10.1021/am3025195 | ACS Appl. Mater. Interfaces 2013, 5, 2325−2330

investigations of solvent vapor annealing using methods such as X-ray scattering have provided more insight, but as demonstrated in this paper, they lack the ablity to relate processing conditions directly to device optimization, because they do not detect dewetting or measure thin film coverage of the substrate. We demonstrate that quartz crystal microbalance with dissipation (QCM-D) is capable of quantifying the uptake of solvent vapor by the film and determining its effect on the thin film, thus allowing it to predict robustly device performance trends in the case of small-molecule semiconductors. Besides proving itself as a powerful process monitoring and optimization tool, QCM-D also reveals key aspects of the mechanism of solvent vapor annealing, namely that keeping the adsorbed solvent molecules isolated is far better for small-molecule OFETs than allowing them to nucleate and form a liquid phase.

■ ASSOCIATED CONTENT

Supporting Information

Raw data of solvent vapor annealed TIPS-Pn thin-films characterized by polarized microscopy and AFM, as well as OTFT transfer and output characteristics with respect to solvent vapor annealing time. This material is available online free of charge at http://pubs.acs.org.This material is available free of charge via the Internet at http://pubs.acs.org.

■ AUTHOR INFORMATION

Corresponding Author

*Tel: +966 (54) 470-0079. E-mail: aram.amassian@kaust.edu.sa.

Author Contributions

‡Authors with equal contribution.

Notes

The authors declare no competing financial interest.

■ ACKNOWLEDGMENTS

Part of this work was supported by KAUST's Office of Competitive Research Funds under Award FIC/2010/04. The authors acknowledge use of the D1 beamline at the Cornell High Energy Synchrotron Source supported by the National Science Foundation (NSF DMR-0936384) and NIH-NIGMS.

■ REFERENCES

(1) Friend, R. H.; Gymer, R. W.; Holmes, A. B.; Burroughes, J. H.; Marks, R. N.; Taliani, C.; Bradley, D. D. C.; Santos, D. A. D.; Brédas, J. L.; Lögdlund, M.; Salaneck, W. R. *Nature* **1999**, *397*, 121.

(2) Wohrle, D.; Meissner, D. *Adv. Mater.* **1991**, *3*, 129.

(3) Steudel, S.; Myny, K.; Arkhipov, V.; Deibel, C.; Vusser, S. D.; Genoe, J.; Heremans, P. *Nature Mater* **2005**, *4*, 597.

(4) Khan, M. A.; Bhansali, U. S.; Alshareef, H. N. *Adv. Mater.* **2012**, *24*, 2165.

(5) Khan, H. U.; Roberts, M. E.; Johnson, O.; Förch, R.; Knoll, W.; Bao, Z. *Adv. Mater.* **2010**, *22*, 4452.

(6) Khan, H. U.; Roberts, M. E.; Johnson, O.; Knoll, W.; Bao, Z. *Org. Electron.* **2012**, *13*, 519.

(7) Bernards, D. A.; Flores-Torres, S.; Abruña, H. D.; Malliaras, G. G. *Science* **2006**, *5792*, 1416.

(8) Bao, Z.; Dodabalapur, A.; Lovinger, A. *J. Appl. Phys. Lett.* **1996**, *69*, 4108.

(9) Minemawari, H.; Yamada, T.; Matsui, H.; Tsutsumi, J.; Haas, S.; Chiba, R.; Kumai, R.; Hasegawa, T. *Nature* **2011**, *475*, 364.

(10) Giri, G.; Verploegen, E.; Mannsfeld, S. C. B.; Atahan-Evrenk, S.; Kim, D. H.; Lee, S. Y.; Becerril, H. A.; Aspuru-Guzik, A.; Toney, M. F.; Bao, Z. *Nature* **2011**, *480*, 504.

(11) Smith, J.; Zhang, W.; Sougrat, R.; Zhao, K.; Li, R.; Cha, D.; Amassian, A.; Heeney, M.; McCulloch, I.; Anthopoulos, T. D. *Adv. Mater.* **2012**, *24*, 2441.

(12) Briseno, A. L.; Mannsfeld, S. C. B.; Ling, M. M.; Liu, S.; Tseng, R. J.; Reese, C.; Roberts, M. E.; Yang, Y.; Wudl, F.; Bao, Z. *Nature* **2006**, *444*, 913.

(13) Rogers, J. A.; Bao, Z.; Baldwin, K.; Dodabalapur, A.; Crone, B.; Raju, V. R.; Kuck, V.; Katz, H.; Amundson, K.; Ewing, J.; Drzaic, P. *Proc. Natl. Acad. Sci. U.S.A.* **2001**, *98*, 4835.

(14) Someya, T.; Dodabalapur, A.; Gelperin, A.; Katz, H. E.; Bao, Z. *Langmuir* **2002**, *18*, 5299.

(15) Yang, S. Y.; Shin, K.; Kim, S. H.; Jeon, H.; Kang, J. H.; yang, H.; Park, C. E. *J. Phys. Chem. B.* **2006**, *110*, 20302.

(16) Rivnay, J.; Jimison, L. H.; Northrup, J. E.; Toney, M. F.; Noriega, R.; Lu, S.; Marks, T. J.; Facchetti, A.; Salleo, A. *Nat. Mater.* **2009**, *8*, 952.

(17) Garnier, F.; Horowitz, G.; Fichou, D.; Yassar, A. *Synth. Met.* **1996**, *81*, 163.

(18) Kline, R. J.; McGehee, M. D.; Kadnikova, E. N.; Liu, J.; Frechet, J. M. J. *Adv. Mater.* **2003**, *15*, 1519.

(19) Lin, Y. Y.; Gundlach, D. J.; Nelson, S. F.; Jackson, T. N. *IEEE Electron Device Lett.* **1997**, *18*, 606.

(20) Minari, T.; Liu, C.; Kano, M.; Tsukagoshi, K. *Adv. Mater.* **2012**, *24*, 299.

(21) Li, R.; Ward, J. W.; Smilgies, D.-M.; Payne, M. M.; Anthony, J. E.; Jurchescu, O. D.; Amassian, A. *Adv. Mater.* **2012**, DOI: 10.1002/adma.201201856.

(22) Dickey, K. C.; Anthony, J. E.; Loo, Y.-L. *Adv. Mater.* **2006**, *18*, 1721.

(23) Akkerman, H. B.; Chang, A. C.; Verploegen, E.; Bettinger, C. J.; Toney, M. F.; Bao, Z. *Org. Electron.* **2012**, *13*, 235.

(24) Amassian, A.; Pozdin, V. A.; Li, R.; Smilgies, D.-M.; Malliaras, G. G. *J. Mater. Chem.* **2010**, *20*, 2623.

(25) Amassian, A.; Pozdin, V. A.; Desai, T. V.; Hong, S.; Woll, A. R.; Ferguson, J. D.; Brock, J. D.; Malliaras, G. G.; Engstrom, J. R. *J. Mater. Chem.* **2009**, *19*, 5580.

(26) Dickey, K. C.; Anthony, J. E.; Loo, Y. L. *Adv. Mater.* **2006**, *18*, 1721.

(27) Mascaro, D. J.; Thompson, M. E.; Smith, H. I.; Bulovic, V. *Org. Electron.* **2005**, *6*, 211.

(28) Chou, K. W.; Yan, B.; Li, R.; Li, E. Q.; Zhao, K.; Anjoum, D. H.; Alvarez, S.; Gassaway, R.; Biocca, A.; Thoroddsen, S. T.; Hexemer, A.; Amassian, A. *Advanced Materials* **2013**, DOI: 10.1002/adma.201203440.

(29) Notley, S. M. *J. Phys. Chem. B* **2008**, *112* (40), 12650.

(30) Schmidt, V.; Giacomelli, C.; Gounou, C.; Lai-Kee-Him, J.; Brisson, A. R.; Borsali, R. *Langmuir* **2008**, *24* (21), 12189.

(31) Fatisson, J.; Domingos, R. F.; Wilkinson, K. J.; Tufenkji, N. *Langmuir* **2009**, *25* (11), 6062.

(32) Harms, H. A.; Tetreault, N.; Gusak, V.; Kasemo, B.; Gratzel, M. *Phys. Chem. Chem. Phys.* **2012**, *14* (25), 9037.

(33) Li, R.; Khan, H. U.; Payne, M. M.; Smilgies, D.-M.; Anthony, J. E.; Amassian, A. *Adv. Funct. Mater.* **2012**, DOI: 10.1002/adfm.201201264.

(34) Sauerbrey, G. *Z. Phys. A: Hadrons Nucl.* **1959**, *155*, 206.

(35) Liu, S. X.; Kim, J. T. *J. Assoc. Lab. Autom.* **2009**, *14* (4), 213.

(36) Ma, H.; Textor, M.; Clark, R. L.; Chilkotia, A. *Biointerphases* **2006**, *1*, 35.

(37) Naderi, A.; Iruthayaraj, J.; Pettersson, T.; Makuška, R.; Claesson, P. M. *Langmuir* **2008**, *24*, 6676.

(38) Lee, S. S.; Loth, M. A.; Anthony, J. E.; Loo, Y.-L. *J. Am. Chem. Soc.* **2012**, *134*, 5436.

(39) He, Z.; Xiao, K.; Durant, W.; Hensley, D. K.; Anthony, J. E.; Hong, K.; Kilbey, S. M.; Chen, J.; Li, D. *Adv. Funct. Mater.* **2011**, *21*, 3617.